RSC Advances

ROYAL SOCIETY OF CHEMISTRY

www.rsc.org/advances

RSC Advances

RSCPublishing

COMMUNICATION

Double-walled TiO_2 nanotubes prepared with NH_4BF_4 based electrolyte and their photoelectrochemical performance

Cite this: DOI: 10.1039/x0xx00000x

Received 00th 2014,
Accepted 00th March 2014

DOI: 10.1039/x0xx00000x

www.rsc.org/ RSC Advances

Hui Li, Junheng Xing, Zhengbin Xia*, Jiangqiong Chen

Highly ordered anodic single-walled TiO_2 nanotubes (SW-TiO_2 NTs) and double-walled TiO_2 nanotubes (DW-TiO_2 NTs) are prepared in the unique NH_4BF_4 based electrolyte. The formation of SW-TiO_2 NTs and DW-TiO_2 NTs can be simply tuned by voltages. The DW-TiO_2 NTs show higher photoelectrochemical performance than the SW-TiO_2 NTs.

Over the past two decades, TiO_2 nanotubes (NTs) prepared by electrochemical anodization method have attracted great attentions in the fields of photocatalysis,[1,2] solar cells,[3-5] sensors[6,7] and Li-ion batteries[8]. Generally, fluoride ions of the aqueous or organic electrolytes are deemed to be the essential ingredient to fabricate anodic TiO_2 NTs.[9-12] However, Schmuki et al. and others recently demonstrated that the self-organized TiO_2 NTs could be also formed in ionic liquid (such as BMIM-BF_4) based electrolytes, which paved a way for the alternative preparation of TiO_2 NTs by using fluoride ions free electrolytes.[13-15] It should be noted that the ionic liquid used in their study was very expensive and the structure of the obtained TiO_2 NTs was irregular, which hindered further development of this method.

The surface area is a crucial factor for the enhancement of photoconversion efficiency of TiO_2 NTs. Double-walled TiO_2 nanotubes (DW-TiO_2 NTs), which possess much higher surface area than the traditional single-walled TiO_2 nanotubes (SW-TiO_2 NTs), are considered to be one of the most promising nanostructures for photoelectrochemical (PEC) applications. Recently, Albu et al. reported the fabrication of obvious DW-TiO_2 NTs through heating processing.[16] Misra et al. fabricated the DW-TiO_2 NTs by sonoelectrochemical anodization using ionic liquid, and the formed DW-TiO_2 NTs showed superb water splitting efficiency.[17] However, in their study, the formed DW-TiO_2 NTs are length limited and disordered, and the anodization system cannot perform well at high voltages. Up to date, no work has been reported on tuning the formation of SW-TiO_2 NTs and DW-TiO_2 NTs in specific electrolyte with effective strategies.

In this paper, we firstly report the fabrication of highly ordered DW-TiO_2 NTs and SW-TiO_2 NTs via two-step anodization method in the NH_4BF_4 based electrolyte rather than in the conventional fluoride ions containing electrolyte. The obtained DW-TiO_2 NTs achieve high photoconversion efficiency of about 0.84% under illumination of stimulated solar light (AM1.5, 100 mW/cm^2).

The two-step anodization is the most convenient method to prepare highly ordered hierarchical top-porous and bottom-tubular TiO_2 nanostructures.[18-21] Fig. 1 shows the SEM and TEM images of the TiO_2 NTs obtained at various voltages. The TiO_2 NTs obtained at 60 V show the obvious dual hierarchical structure. Holes with average diameter (D) of about 40 nm are uniformly distributed in the upper layer (Fig. 1a) and the topology of the bottom layer displays the apparent double-walled structure with the inner porediameter of 40 nm, outer porediameter of 100 nm, and the length of around 800 nm (Fig .1b). The double-walled TiO_2 NTs can be also found in TEM image (Fig .1c). For the TiO_2 NTs formed at 80 V, the nanopores diameter (D=50 nm) of the upper layer increases with voltages (Fig. 1d), and the bottom tubular layer shows the single-wall/double-wall combined transition state. The thickness of bottom layer is about 2 μm with the internal diameter, external diameter of 50 nm, 100 nm separately (Fig. 1e), which is in accordance with the TEM image (Fig .1f). The results suggest that the length of the TiO_2 NTs increases with potentials, which is consistent with the reports that the nanotubes length is proportional to the applied voltages for the same anodization duration.[22,23] The hexagonal pores size (D=120 nm) increases as the voltages increases to 100 V (Fig. 1g), and the bottom layer shows the obvious single-walled structure with the nanopores diameter of 150 nm and the tube length of approximately 2.5 μm (Fig. 1h). In TEM image the single wall thickness of 8 nm can be directly observed (Fig .1i). In short, these results show that it can easily control the transformation of the TiO_2 NTs from double-wall to single-wall by tuning the applied voltages.

Fig. 2a shows the XRD results of the unannealed and annealed samples. The unannealed sample prepared at 80 V is amorphous, while the samples formed at various potentials and were subsequently annealed at 450 ^oC for 2 h present the anatase phases. Fig. 2b reveals the double peaks at 458.6 and 464.3 eV, corresponding to the Ti $2p_{3/2}$ and Ti $2p_{1/2}$ of the Ti^{4+} (TiO_2), respectively.[24] The O 1s XPS peak of the formed TiO_2 NTs in Fig. 2c can be separated with two distinct peaks, the dominant peak at 529.7 eV is in agreement with O 1s electron binding energy for TiO_2, whereas the weak peak at 531.3 eV suggests the formation of F-Ti-O or N-Ti-O structures.[25] As shown in Fig. 2d, the presence of a broad peak around 400.09 eV implies the state of the doped nitrogen TiO_2.[26,27] Fig. 2e shows a single peak of B 1s at 192.4 eV, which is attributed to Ti-O-B interstitial boron.[28,29] A pair of peaks at

685.1 and 688.7 eV are observed for F 1s (Fig. 2f), which can be assigned

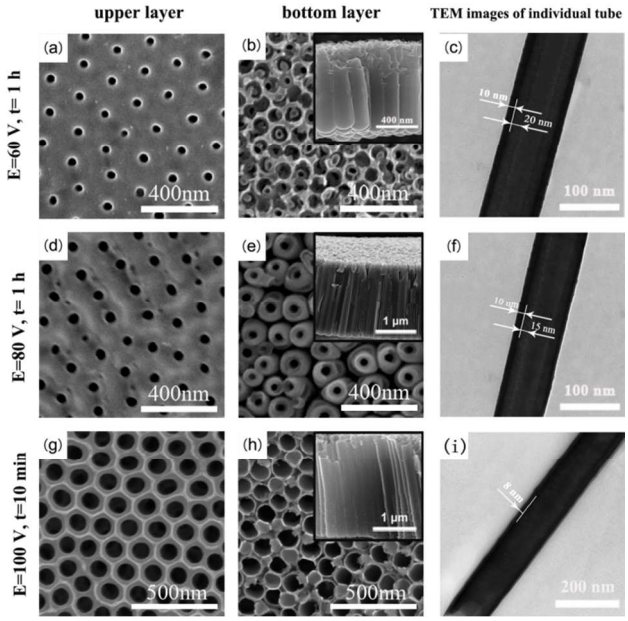

Fig. 1 SEM images of the upper layer, the bottom layer and TEM images of TiO_2 NTs grown at: 60 V (a, b, c), 80 V (d, e, f) and 100 V (g, h, i). The upright insets in (b), (e) and (h) show the cross-sectional views of the corresponding TiO_2 NTs.

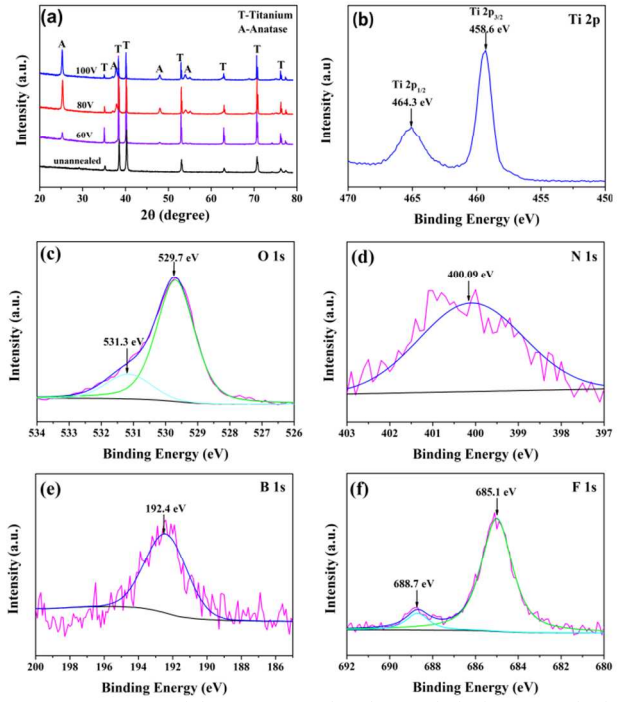

Fig. 2 XRD patterns of the as-prepared and annealed TiO_2 NTs obtained at different voltages unannealed and annealed in oxygen at 450 ºC for 2 h (a), and Ti 2p (b), O 1s (c), N 1s (d), B 1s (e), F 1s (f) XPS spectra of TiO_2 NTs prepared at 80 V for 1 h.

to the metal-fluoride bonding such as Ti-F and the doped F atoms in the TiO_2 matrix, respectively.[30-32] To sum up, the XPS results reveal that the nonmetal elements of N, F and B are doped into the obtained TiO_2 NTs.

The UV-vis diffuse reflectance absorption spectra (DRS) of as-prepared samples are shown in Fig. 3. The slightly red shifts of the absorption edge are observed for the prepared samples compared with the reported pure anatase TiO_2 (about 400 nm), indicating the band gaps of all samples are definitely narrowed, which may be due to the anion (N, F and B) doping effect discussed in the above XPS. Moreover, the DW-TiO_2 NTs show much higher light absorption in visible light region than the SW-TiO_2 NTs. This is ascribed to the DW-TiO_2 NTs possess larger specific surface area in comparison with the SW-TiO_2 NTs for effective light trapping. It is worth noting that the absorbance in the visible region of the DW-TiO_2 NTs formed at 80 V (DW_{80V}-TiO_2 NTs) is stronger than that of the DW-TiO_2 NTs formed at 60 V (DW_{60V}-TiO_2 NTs). The enhanced ability of the DW-TiO_2 NTs to absorb visible light makes it a promising photocatalyst for solar-driven applications.

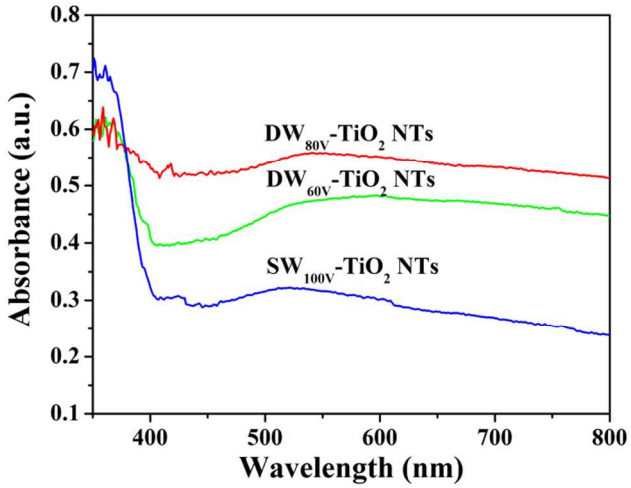

Fig. 3 UV-vis diffuse reflectance spectra of DW_{60V}-TiO_2 NTs, DW_{80V}-TiO_2 NTs and SW_{100V}-TiO_2 NTs.

Prior to the PEC measurements, the thin upper layer of the samples were ultrasonically removed for simply discussing the influences of single-walled and double-walled structures on the PEC performance of TiO_2 NTs. Fig. 4a shows that the photocurrent of the DW-TiO_2 NTs formed at the voltages of 80 V and 60 V are much higher than that of the SW-TiO_2 NTs fabricated at the voltage of 100 V, which means that the photoresponse and the charge transport properties of the DW-TiO_2 NTs are better than that of the SW-TiO_2 NTs. Moreover, as shown in Fig. 4b, the photocurrent density of the DW_{80V}-TiO_2 NTs, DW_{60V}-TiO_2 NTs is 1.60 and 0.96 mA/cm^2 at 1.23 V (vs. RHE), about 166% and 60% higher than that of the SW_{100V}-TiO_2 NTs. The DW_{80V}-TiO_2 NTs show more excellent PEC performance than the DW_{60V}-TiO_2 NTs, due to that the DW_{80V}-TiO_2 NTs possess much more aligned tubular structure than the DW_{60V}-TiO_2 NTs, which can reduce the recombination of the electrons and holes.

The hydrogen production efficiency of the obtained TiO_2 NTs is calculated via the following equation:[33]

$$\varepsilon_0(\%) = j_p \frac{E^0_{rev} - |E_{app}|}{I_0} \times 100$$

where ε_0 is the photoconversion efficiency, j_p is the photocurrent density (mA/cm^2), I_0 means the intensity of the incident light, E^0_{rev} represents the standard reversible potential (1.23 V vs. RHE), and $|E_{app}|$ denotes the absolute value of the applied voltage which is obtained from $E_{app} = E_{meas} - E_{aoc}$, where E_{meas} is the electrode potential (vs. Ag/AgCl) at which j_p is measured and E_{aoc} is the electrode potential (vs. Ag/AgCl) at open circuit under illumination. Plots of photoconversion

efficiency with applied potential are shown in Fig. 4c. The DW_{80V}-TiO_2 NTs, DW_{60V}-TiO_2 NTs, SW_{100V}-TiO_2 NTs show maximum efficiencies of 0.84%, 0.46%, 0.25% at 0.8 V (vs. RHE), respectively, which means that the DW-TiO_2 NTs show better photocatalysis performance than the SW-TiO_2 NTs. A possible explanation for this is that the DW-TiO_2 NTs have larger surface area, more porous structure and better light absorption in comparison with the SW-TiO_2 NTs.

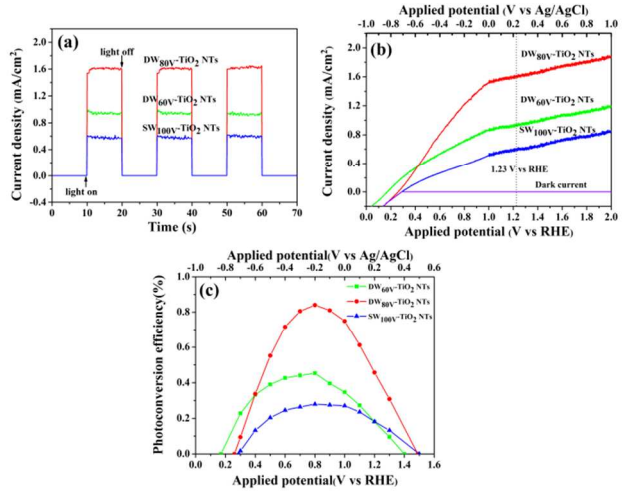

Fig. 4 Photoelectrochemical properties of DW_{60V}-TiO_2 NTs, DW_{80V}-TiO_2 NTs, SW_{100V}-TiO_2 NTs electrodes: amperometric I-t curves at an applied potential of 1.23 V (vs. RHE) (a), linear-sweep voltammograms with scanning rate of 5 mV/s (b), and photoconversion efficiency as a function of applied potentials (c).

To understand the bulk diffusion and surface charge transfer characteristics and reveal the differences in the PEC activity of the as-prepared samples, photoluminescence (PL) technique has been used to determine the efficiency of charge carriers trapping, migration and transfer due to the PL signals of the semiconductor materials, resulting from the recombination of photoexcited charge carriers.[34,35] As shown in Fig. 5, all samples display PL peaks at around 420 nm. The PL intensity of DW_{80V}-TiO_2 NTs and DW_{60V}-TiO_2 NTs are all much slower than that of the SW_{100V}-TiO_2 NTs. These results demonstrate that the double-walled structure effectively inhibits the photoexcited charge recombination. Furthermore, the DW_{80V}-TiO_2 NTs exhibit a weaker PL intensity compared with the DW_{60V}-TiO_2 NTs. It can be attributed to that the well ordered structure of DW_{80V}-TiO_2 NTs facilitate the separation of electron-hole pairs.

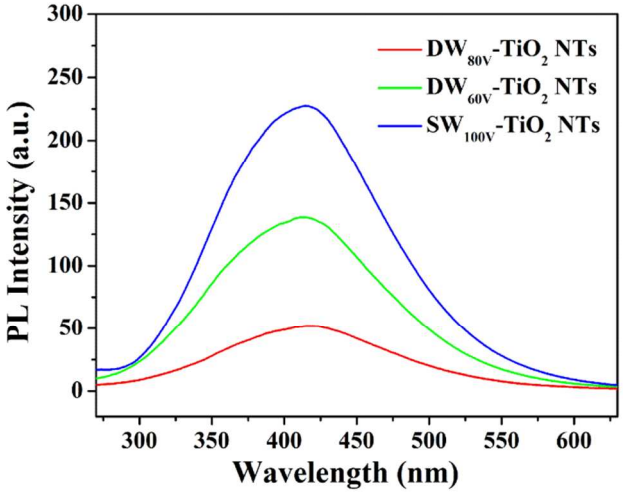

Fig. 5 Photoluminescence (PL) spectra of DW_{60V}-TiO_2 NTs, DW_{80V}-TiO_2 NTs and SW_{100V}-TiO_2 NTs.

The mechanisms of the formation of the DW-TiO_2 NTs and SW-TiO_2 Ns prepared at various anodizing voltages in the NH_4BF_4 based electrolyte is discussed briefly. Firstly, the anion BF_4^- are partly decomposed to release the fluoride ions into the electrolyte under the high electric field. Subsequently, two types of pitting take place on the well-textured Ti surface during the initial stage of the second-step of anodization process because of the different etching ability of the BF_4^- and F^-.[17] The electric field distribution in the curved bottom of the imprint pores is larger than that in the edge of the concave holes, which causes the decomposed F^- enrich in the bottom rather than in the fringe of the pore (fig. 6a). The produced F^- are more prone to react with Ti and TiO_2 at the centre of the concavity than BF_4^-, thus the bottom pore grows deeper with the fast etching rate of F^-, meanwhile, the voids occur at the surrounding walls of the pores and continue grow to be tubes with the slow etching rate of BF_4^-.Thereafter, the double-walled NTs which consist of longer inner tubes and shorter outer tubes are formed with the different etching rate of the F^- and BF_4^- (Fig. 6b). The amount of free fluoride ions may depends on the applied potentials, which means that high anodizing voltages (100 V) generate more fluoride ions than the low potentials (60 V), therefore the formed double-walled

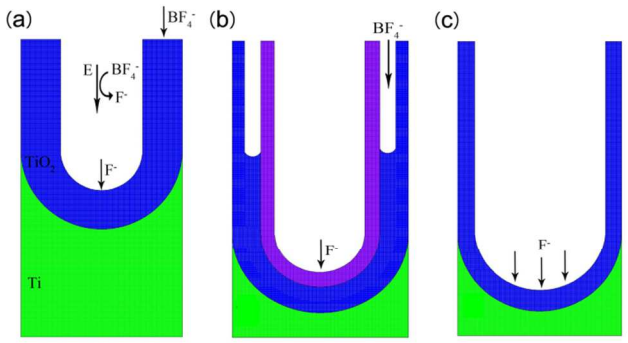

structure at low potentials is relatively stable, while it disappears due to the intensive dissolution of F^- dissociated at high voltages to form the thin single-walled structure (Fig. 6c).

Fig. 6 Schematic diagram of DW-TiO_2 NTs and SW-TiO_2 NTs formation by two-step anodization in the NH_4BF_4 based electrolyte. Initial stage of the second-step of anodization process (a), DW-TiO_2 NTs (b) and SW-TiO_2 NTs (c) formed at low and high potentials, respectively.

In summary, we investigate the fabrication of uniform TiO_2 NTs in NH_4BF_4 based electrolyte. DW-TiO_2 NTs, combined DW-TiO_2/SW-TiO_2 NTs and SW-TiO_2 NTs are obtained at 60 V, 80 V and 100 V, respectively. The DW-TiO_2 NTs possess larger surface area and better orderliness than the SW-TiO_2 NTs, which result in higher photocurrent and photoconversion efficiency. We believe our discovery is significant in that it allows us to use a previously unexplored anodizing electrolyte for the synthesis of TiO_2 NTs and presents a new avenue to fabricate the DW-TiO_2 NTs for improving photoconversion efficiency in PEC water splitting performance.

We acknowledge the financial support from the National Nature Science Foundation of China (NSFC, NO. 20976058).

Notes and references

School of Chemistry and Chemical Engineering, South China University of Technology, Guangzhou 510641, China.
E-mail: cezhbxia@scut.edu.cn; Fax: +86 20 8711 2093;
Tel.: +86 20 8711 2047

†Electronic Supplementary Information (ESI) available: Experimental methods, photoelectrochemical activity tests. See DOI: 10.1039/c000000x.

1 S. P. Albu, A. Ghicov, J. M. Macak, R. Hahn and P. Schmuki, *Nano Lett*., 2007, **7**, 1286.
2 C. J. Lin, W. Y. Yu, Y. T. Lu and S. H. Chien, *Chem. Commun*., 2008, **45**, 6031.
3 B. O'Regan and M. Grätzel, *Nature*, 1991, **353**, 737.
4 J. M. Macak, H. Tsuchiya, A. Ghicov and P. Schmuki, *Electrochem. Commun*., 2005, **7**, 1133.
5 Q. W. Chen and D. S. Xu, *J. Phys. Chem. C*, 2009, **113**,6310.
6 O. K. Varghese, D. W. Gong, M. Paulose, K. G. Ong, E. C. Dickey and C. A.Grimes, *Adv. Mater*., 2003, **15**, 624.
7 G. K. Mor, O. K. Varghese, M. Paulose and C.A. Grimes, *Sens. Lett*., 2003, **1**, 42.
8 H. Q. Li, S. K. Martha, R. R. Unocic, H. M. Luo, S. Dai and J. Qu, *J. Power Sources*, 2012, **218**, 88.
9 D. Gong, C. A. Grimes, O. K. Varghese, W. Hu, R. S. Singh, Z. Chen and E.C. Dickey, *J. Mater. Res*., 2001, **16**, 3331.
10 Q. Y. Cai, M. Paulose, O. K. Varghese and C. A. Grimes, *J. Mater. Res*., 2005, **20**, 230.
11 M. Paulose, K. Shankar, S. Yoriya, H. E. Prakasam, O. K. Varghese, G. K. Mor, T. J. LaTempa, A. Fitzgerald and C. A. Grimes, *J. Phys. Chem. B*, 2006, **110**, 16179.
12 N. K. Allam and C. A. Grimes, *J. Phys. Chem. C*, 2007, **111**, 13028.
13 I. Paramasivam, J. M. Macak, T. Selvam and P. Schmuki, *Electrochim. Acta*., 2008, **54**, 643.
14 H. Q. Li, J. Qu, Q. Z. Cui, H. Xu, H. M. Luo, M. F. Chi, R. A. Meisner, W. Wang and S. Dai, *J. Mater. Chem*., 2011, **21**, 9487.
15 H. Wender, A. F. Feil, L. B. Diaz, C. S. Ribeiro, G. J. Machado, P. Migowski, D. E. Weibel, J. Dupont and S. R. Teixeira, *ACS Appl. Mater. Interfaces*, 2011, **3**, 1359.
16 S. P. Albu, A. Ghicov, S. Aldabergenova, P. Drechsel, D. LeClere, G. E. Thompson, J. M. Macak and P. Schmuki, *Adv. Mater*., 2008, **20**, 4135.
17 S. E. John, S. K. Mohapatra and M. Misra, *Langmuir*, 2009, **25**, 8240.
18 J. M. Macak, S. Albu, D. H. Kim, I. Paramasivam, S. Aldabergerova and P. Schmuki, *Electrochem. Solid-State Lett*., 2007, **10**, K28.
19 S. Q. Li, G. M. Zhang, D. Z. Guo, L. G. Yu and W. Zhang, *J. Phys. Chem. C*, 2009, **113**, 12759.
20 D. S. Guan and Y. Wang, *Nanoscale*, 2012, **4**, 2968.
21 Z. H. Zhang and P. Wang, *Energy Environ. Sci*., 2012, **5**, 6506.
22 H. E. Prakasam, K. Shankar, M. Paulose and C. A. Grimes, *J. Phys. Chem. C*, 2007, **111**, 7235.
23 S. Yoriya, M. Paulose, O. K. Varghese, G. K. Mor and C. A. Grimes, *J. Phys. Chem. C*, 2007, **111**, 13770.
24 J. H. Xing, H. Li, Z. B. Xia, J. F. Hu, Y. H. Zhang and L. Zhong, *J. Electrochem. Soc*., 2013, **160**, C503.
25 J. C. Yu, L. Z. Zhang, Z. Zheng and J. C. Zhao, *Chem. Mater*., 2003, **15**, 2280.
26 G. Liu, F. Li, D. W. Wang, D. M. Tang, C. Liu, X. Ma, G. Q. Lu and H. M. Cheng, *Nanotechnology*, 2008, **19**, 025606.
27 D. H. Wang, L. Jia, X. L. Wu, L. Q. Lu and A. W. Xu, *Nanoscale*, 2012, **4**, 576.
28 X. S. Zhou, F. Peng, H. J. Wang, H. Yu and J. Yang, *J. Solid State Chem*., 2011, **184**, 134.
29 X. S. Zhou, F. Peng, H. J. Wang, H. Yu and J. Yang, *Electrochem. Commun*., 2011, **13**, 121.
30 A. Suzuki, Y. Shinka and M. Masuko, *Tribol Lett*., 2007, **27**, 307.
31 W. Ho, J. C. Yu and S. Lee, *Chem. Commun*., 2006, **10**, 1115.
32 Q. Li and J. K Shang, *Environ. Sci. Technol*., 2009, **43**, 8923.
33 S.U.M. Khan, M. Al-Shahry and W. B. Ingler Jr, *Science*, 2002, **297**, 2243.
34 J. C. Yu, J. G. Yu, W. K. Ho, Z. T. Jiang and L. Z. Zhang, *Chem. Mater*., 2002, **70**. 3808.
35 Y. Cong, J. L. Zhang, F. Chen, M. Anpo and D. N. He, *J. Phys. Chem. C*, 2007, **111**, 10618.

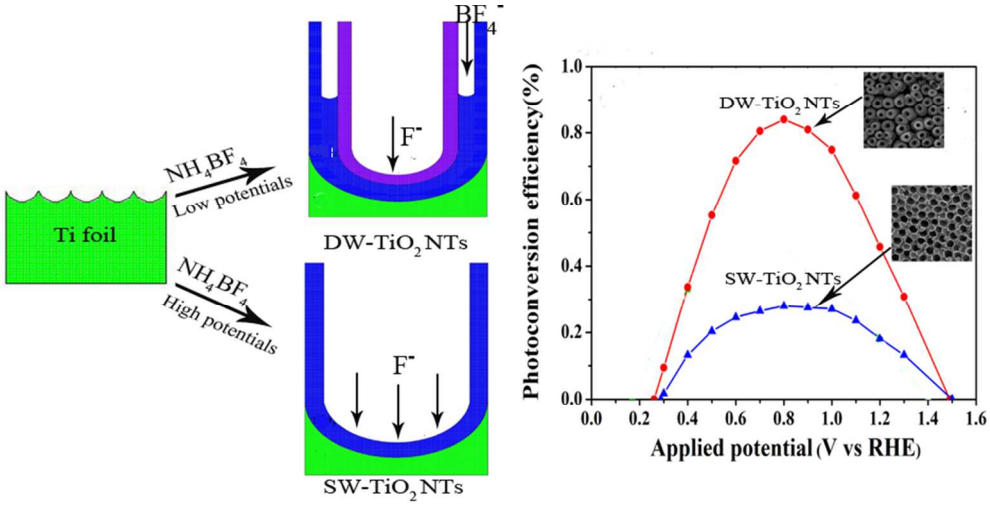

Anodic DW-TiO2 NTs and SW-TiO2 NTs are prepared in NH4BF4 based electrolyte and their formation can be tuned by voltages.
80x39mm (300 x 300 DPI)